UDK 620.1:621.35:621.35
Original scientific article/Izvirni znanstveni članek

ISSN 1580-2949
MTAEC9, 54(2)233(2020)

FACILE SYNTHESIS OF $Co(OH)_2$/RGO/NF ELECTRODES WITH A POROUS NANOSTRUCTURE FOR HIGH-PERFORMANCE SUPERCAPACITORS

ENOSTAVNA SINTEZA POROZNIH NANOSTRUKTURIRANIH $Co(OH)_2$/RGO/NF ELEKTROD ZA VISOKOKAKOVOSTNE SUPERKONDENZATORJE

Zhongjie Lu, Jun Li*, Wanli Jia, Yunqiang Jiang, Yongfei Juan

School of Materials Engineering, Shanghai University of Engineering Science, Shanghai, 201620, China

Prejem rokopisa – received: 2019-05-06; sprejem za objavo – accepted for publication: 2019-10-14

doi:10.17222/mit. 2019.093

$Co(OH)_2$ nanosheets with a high specific capacitance were successfully electrodeposited on nickel foam (NF) covered with reduced graphene oxide (RGO) prepared by electrophoretic deposition followed by thermal reduction. The evolution in the morphology of the deposits with the change in deposition potential was investigated in detail. Moreover, the electrochemical performance of the electrodes was also measured by cyclic voltammetry (CV) and galvanostatic charge/discharge. The relationship between the morphology and the electrochemical performance was also established. The evolution in the morphology of the deposits with the applied potential was described as follows: coarse nanosheets with a low density at –0.75 V (many pores were distributed among them) →fine nanosheets with a comparatively high density at -0.85 V (a large number of pores were located among them) →a very compact structure resulting from the overgrowth and connection among nanosheets (the pores were hardly observed). The $Co(OH)_2$/RGO/NF electrode prepared at –0.85 V demonstrated the highest specific capacitance at a low charge-discharge rate (1503.8 $F \cdot g^{-1}$ and 15.2 $F \cdot cm^{-2}$ at 3 $mV \cdot s^{-1}$ for CV, 1277.5 $F \cdot g^{-1}$ and 12.9 $F \cdot cm^{-2}$ at 1 $A \cdot g^{-1}$ for galvanostatic charge/discharge) when compared with those prepared at –0.75 V and –0.95 V. The electrode prepared at –0.85 V also exhibited an excellent cycling stability, about 83 % of the initial specific capacitance was maintained after 2000 cycles.

Keywords: $Co(OH)_2$, graphene, electrochemical deposition, electrophoretic deposition, supercapacitors

Avtorji so uspešno nanesli tanke $Co(OH)_2$ nanoploščice z visoko kapacitivno upornostjo na nikljevo peno (NF), prekrito z reduciranim grafen oksidom (RGO). Postopek so izvedli z elektrodepozicijo, ki ji je sledila še termična redukcija. Natančno so raziskali razvoj in morfologije nanosov (s SEM, XRD in XPS) glede na spremembo depozicijskega potenciala. Nadalje so elektrokemične lastnosti elektrod določili s ciklično voltametrijo (CV) in galvanostatično naelektrivijo oz. razelektritvijo. Ugotovili so povezavo med morfologijo in elektrokemičnimi lastnostmi. Opisali so razvoj morfologije nanosov glede na uporabljeni potencial. Pri –0,75 V so nastale grobe nanoploščice z nizko gostoto (veliko relativno velikih por je bilo razporejenih med njimi). Pri potencialu –0,85 V so nastale fine nanoploščice (veliko število malih por je bilo lociranih med njimi) katerim je sledila zelo kompaktna struktura s pretirano rastjo in povezavo med nanoploščicami (pore je bilo težko zaznati). $Co(OH)_2$/RGO/NF elektrode izdelane pri –0,85 V so imele najvišjo specifično kapacitanco pri nizkem razmerju med naelektritvijo in razelektritvijo (1503,8 $F \cdot g^{-1}$ in 15,2 $F \cdot cm^{-2}$ pri 3 $mV \cdot s^{-1}$ za CV, 1277,5 $F \cdot g^{-1}$ in 12,9 $F \cdot cm^{-2}$ pri 1 $A \cdot g^{-1}$ za galvanostatično naelektritev/razelektritev) v primerjavi s tistimi, ki so bile pripravljene pri potencialu -0,75 V oz. –0,95 V. Elektrode pripravljene pri –0,85 V so prav tako imele odlično ciklično stabilnost; to je: ohranile so približno 83 % začetne specifične kapacitance po 2000 ciklih.

Ključne besede: $Co(OH)_2$, grafen, elektrokemična depozicija, elektroforeza, superkondenzatorji

1 INTRODUCTION

With the advent of the global energy crisis, a large number of researchers have devoted themselves to the development of new energy-conversion and storage devices.[1,2] Supercapacitors are regarded as a promising energy-storage and conversion device due to their high power density, high specific capacitance, long cycle life and preeminent charge–discharge rate performance.[3–6] Based on the charge-storage mechanism, supercapacitors are usually divided into two categories, corresponding to electrical double layer capacitors (EDLCs) and pseudo-capacitors. Carbon-based materials are regarded as the most popular electrode materials for EDLCs, in which the charges are stored in the double electrode layer and separated at the interface between the electrode and the electrolyte. Transition-metal oxides (or hydroxides)/conducting polymers as the promising electrode materials are frequently applied in pseudo-capacitors, in which the charges are involved in the electrode by fast and reversible redox reactions. A large number of investigations have confirmed that the electrochemical performance of supercapacitors is closely related to the characteristics of the electrode materials.[7–9]. Over past years, a considerable number of investigations into selection and exploration of the electrode materials were carried out (especially transition-metal oxides/hydroxides due to their higher energy).

*Corresponding author's e-mail:
jacob_lijun@sues.edu.cn (Jun Li)

Cobalt hydroxide ($Co(OH)_2$), as an electrode material for pseudo-capacitors, has attracted widespread concerns because of its high energy density, good electrical properties and high theoretical specific capacity (3460 $F \cdot g^{-1}$).[10–12] However, its inherent low conductivity greatly reduces the charge transportation rate, which deteriorates its rating capability. On the other hand, its high self-aggregation tendency also significantly decreases the specific surface area for the charge exchange and prolongs the diffusion path of the charges, resulting in an actual specific capacitance far below the theoretical value and with the rating capability seriously weakened. Moreover, the drastic volume change during the cycling also exacerbates the breakage/pulverization susceptibility, leading to a violent capacity decay in the charge-discharge cycles. The above-mentioned shortcomings can be solved to a certain extent by a special structure design, namely, introducing a flexible material with a large specific surface area and a high electrical conductivity into $Co(OH)_2$. The combination will endow the composite electrode with an excellent electrochemical performance due to its tremendous and short active diffusion channels, and good tolerance to volume change in the charge-discharge process. Graphene with a two-dimensional ultrathin structure is regarded as an ideal candidate for carrying $Co(OH)_2$ due to its large specific surface area, high electrical conductivity and good structural flexibility.

$Co(OH)_2$/graphene composites have been prepared as electrode materials for supercapacitors using different strategies. C. M. Zhao et al.[13] prepared vertically aligned graphene nanosheets by chemical vapor deposition (CVD) on nickel foam (NF) current collectors as substrates and subsequently synthesized $Co(OH)_2$ nanosheets on graphene/NF by electrodeposition in a $Co(NO_3)_2$ aqueous solution. The electrode exhibited a specific capacitance of 693.8 $F \cdot g^{-1}$ at a current density of 2 $A \cdot g^{-1}$ in a potential range of –0.1–0.45 V. U. M. Patil et al.[14] also firstly synthesized porous, lightweight, conducting 3D multilayered graphene on NF by CVD, then produced $Co(OH)_2$ by electrodeposition. A high specific capacitance of 1030 $F \cdot g^{-1}$ was obtained at a current density of 9.09 $A \cdot g^{-1}$. Y. Q. Zhang et al.[15] synthesized a $Co(OH)_2$-graphene composite in a mixture of graphene oxide (GO), $Co(NO_3)_2$, ammonia and hydrazine hydrate through a simultaneous hydrothermal method. The electrochemical measurements showed that the specific capacitances of the pure $Co(OH)_2$ and the $Co(OH)_2$/GO composite are 1186 $F \cdot g^{-1}$ and 1598 $F \cdot g^{-1}$ at a scan rate of 5 $mV \cdot s^{-1}$, respectively. E. M. Jin et al.[16] prepared the $Co(OH)_2$/graphene composite via a two-step method. The commercial graphene nanosheet (GNS) was mixed into acetylene black and polyvinylidene fluoride (PVDF) at a mass ratio of 100:15:10 in N-methyl pyrrolidinone (NMP), and then pasted onto a Ti-mesh. Finally, $Co(OH)_2$ was electrodeposited on the Ti-mesh carrying GNS using chrono-amperometric techniques. The power and energy densities of the $Co(OH)_2$/GNS electrode were 1137 $W \cdot k\ g^{-1}$ and 43 $Wh \cdot k\ g^{-1}$ at 8 $mA \cdot cm^{-2}$, respectively. Present investigations have confirmed that the introduction of graphene into $Co(OH)_2$ is an effective strategy for the improvement in electrochemical performance of $Co(OH)_2$.

In this study, $Co(OH)_2$/RGO (reduced graphene oxide) composites as the electrode materials of supercapacitors were synthesized by a new two-step method. RGO was firstly deposited on NF using electrophoretic deposition, followed by thermal reduction. Then, $Co(OH)_2$/RGO composites were produced by electrochemically depositing $Co(OH)_2$ nanosheets on RGO/NF. Electrophoretic deposition followed by thermal reduction is considered as an economical and versatile alternative for fabricating RGO films with controllable thickness and morphology on different substrates.[17–24] The morphology and thickness of $Co(OH)_2$ deposited on RGO can be flexibly regulated in electrochemical deposition by changing the deposition variables such as electrolyte, deposition potential, temperature and time. The integration of the above-mentioned methods will provide a novel synthesis route for $Co(OH)_2$/RGO composites with excellent electrochemical performance. The evolution in morphology of $Co(OH)_2$ with the applied potentials was investigated in detail. The cyclic voltammetry (CV) and galvanostatic charging/discharging techniques were applied to investigate the effect of the morphological evolution on the electrochemical performance of the composite electrode materials. The relationships among the potential, $Co(OH)_2$ morphology and the electrochemical performance were established, based on which a suitable potential was confirmed.

2 EXPERIMENTAL PART

2.1. Synthesis of reduced graphene oxide (RGO)

Nickel foam (NF) pieces (Shanxi Power Source Battery Materials Co., Ltd., Taiyuan, Shanxi, China) with a size of 20 mm × 20 mm × 0.5 mm were selected as the current collectors, which were ultrasonically cleaned with acetone, 1 $mol \cdot L^{-1}$ HCl and distilled water for 20 min. Then they were dried in a DZF-6020 vacuum drying oven (Shanghai Jinghong Experimental Equipment Co., Ltd) at 30 °C for 8 h, and weighed using a Sartorius SQP electronic balance with an accuracy of 0.01 mg (Sartorius Instruments Co., Ltd. Beijing. China).

The electrophoretic deposition of graphene oxide (GO) was carried out on a WYJ-150V3A direct-current stabilized-voltage power supply coupled with a plating bath (Shanghai Wenkai Power equipment Co., Ltd., China). Two pieces of graphite were symmetrically placed on the two sides of a piece of NF with about 1 cm space left between them, which were immersed in a 0.5 $mol \cdot L^{-1}$ GO solution. Then, GO was deposited at an applied potential of 60 V for 60 s. The GO/NF pieces were naturally dried in air after deposition and then

sintered in argon at 300 °C for 2 h, during which time the GO was successfully transformed into RGO. The RGO/NF pieces were weighed again to obtain the RGO weight by subtracting the NF weight.

2.2. Electrodeposition of $Co(OH)_2$ on RGO/NF

$Co(OH)_2$ was prepared on RGO/NF by electrodeposition in an aqueous solution containing 0.5 mol·L^{-1} cobalt nitrate [$Co(NO_3)_2$] and 0.075 mol·L^{-1} sodium nitrate ($NaNO_3$) on a CHI 6082D electrochemical workstation (ChenHua Instruments Ins, Shanghai, China). The applied potential is very critical for the deposits, which can be determined by cyclic voltammetry (CV). **Figure 1** indicates the CV curve recorded on RGO/NF in the above electrolyte at a scanning rate of 5 mV·s^{-1}. It is clear that the current is rapidly increased when the potential is more negative than –0.65 V, which indicates that $Co(OH)_2$ begins to be deposited on RGO/NF. Therefore, the potentials of –0.75 V, –0.85 V and –0.95 V were applied for 30 min. The conventional three-electrode system was adopted, in which the RGO/NF piece, the graphite piece and the saturated calomel electrode were selected as the working, counter and reference electrodes, respectively. The working electrodes were weighed again to obtain the weight of $Co(OH)_2$ by subtracting the weight of RGO/NF. The amount of deposited RGO and $Co(OH)_2$ is small when compared with that of NF (about 0.1 % and 2 % of that of NF), so that the weight measurement errors can be generated before and after depositing RGO and $Co(OH)_2$. This will subsequently cause calculation errors in terms of the specific capacitance of the electrode. In order to ensure high data accuracy and good result reproducibility, all the samples were strictly treated by the same route and three parallel samples were prepared under the same experimental conditions. Moreover, for a given sample, the depositing amount of RGO and $Co(OH)_2$ will be weighed three times using a high-resolution electronic balance. Then, the average values were obtained to calculate the weight of deposited RGO and $Co(OH)_2$. Besides those, the electrochemical performance was also measured three times in the CV and galvanostatic charge–discharge tests to obtain excellent reproducibility. The specific capacitance of $Co(OH)_2$ was calculated based on the measured electrochemical results.

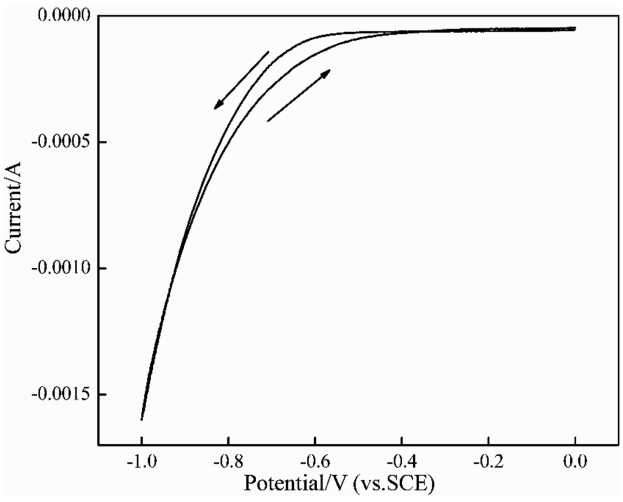

Figure 1: CV curves recorded on RGO/NF at a scanning rate of 5 mV·s^{-1}

2.3. Structural characterization

The morphologies of the deposits prepared at different potentials (–0.75 V, –0.85 V, –0.95 V) were characterized in detail using a Hitachi S-4800 scanning electron microscope (SEM, Tokyo Hitachi Co., Ltd.). Phase constituents of the deposit at –0.85 V were identified by an X'Pert Pro X-ray diffractometer (XRD, PANalytical, Eindhoven, Netherlands) with Cu-K_α radiation (λ = 0.1540560 nm). The chemical valence states of Co in the deposit at –0.85 V were identified by an X-ray photoelectron spectroscope (XPS, Escalab 250xi, Thermo Fisher Science, Massachusetts, America) with a monochrome Al-K_α source. An energy step size of 0.1eV was selected for the spectral analysis. The binding energy scale is based on the C1s peak (781 eV) of Co on the surface of analytical samples.

2.4. The tests for electrochemical performance of $Co(OH)_2$/RGO/NF electrodes

The electrochemical performance of $Co(OH)_2$/NF and $Co(OH)_2$/RGO/NF electrodes was measured using CV and galvanostatic charge/discharge tests on a CHI 6082D electrochemical workstation (ChenHua Instruments Ins, Shanghai, China) in a 2 mol·L^{-1} KOH aqueous solution. Similarly, a conventional three-electrode system was adopted, in which the $Co(OH)_2$/NF and $Co(OH)_2$/RGO/NF piece, the graphite piece and the saturated calomel electrode were selected as the working, counter and reference electrodes, respectively. CV tests were carried out in the potential range from –0.2 V to 0.5 V at scanning rates of (3, 5, 7, 9) mV·s^{-1}, galvanostatic charge/discharge tests were performed in the potential range of –0.1 V to 0.45 V at a current density of (1.0, 1.5, 2.0, 2.5, 4.0) A·g^{-1}, respectively. A total of 2000 CV cycles were used to test the cycle performance at a scanning rate of 5 mV·s^{-1}.

3 RESULTS AND DISCUSSION

3.1. Structural characterization

Figure 2 shows the XRD patterns of the RGO/NF samples before and after the electrodeposition. Prior to the electrodeposition, three strong peaks can be clearly identified at 2θ = 44.6°, 51.9° and 76.4° in two XRD patterns. By comparing their d values with those in the JCPDS cards, they derive from the diffraction of (111), (200) and (220) planes related to Ni from NF (JCPDS

card NO.04-0850). A clear inspection reveals that a very weak broad peak can be observed at near 24°, confirming the existence of RGO. It can be concluded that a thin layer of RGO was successfully synthesized by electrophoretic deposition, followed by thermal reduction. The XRD pattern presents the significant change for the sample subjected to the electrodeposition. Besides the three strong peaks associated with Ni and a weak peak from RGO, the other three peaks appear at around 2θ = 19.5°, 2θ = 32.9° and 2θ = 58.8°. The indexed result indicates that their d values agree well with those of α-$Co(OH)_2$ (JCPDS card NO.46-0605), which means that α-$Co(OH)_2$ is well electrodeposited on RGO/NF.

XRD does not belong to the group of surface-analysis methods. So it cannot be used to precisely identify the phase constituents of the thin layer of deposits prepared in this study due to serious interference from the substrate (NF). Only the main phases involved in the deposits can be identified, some tiny phases with the volume fraction of less than 5 % cannot be precisely confirmed. Moreover, different phases in the deposits are difficult to be quantitatively analyzed. Compared with XRD, XPS is a surface-analysis technique with an analysis depth of less than 10 nm and a low analyzed limit of element concentration (<0.1 *a*/%), which is suitable to analyze the relative contents and chemical valence states of different elements in the deposits. The interference from the substrate elements can be effectively eliminated, and the tiny amounts of elements can also be precisely detected. The relative contents of the different phases can be further determined based on the elemental contents. **Figure 3** indicates the high-resolution narrow spectrum of Co_{2p}. Four peaks can be fitted into three groups of peaks marked with three kinds of color. Two peaks located at 781.3 eV and 798.0 eV in the first group confirm the existence of $Co_{2p3/2}$ and $Co_{2p1/2}$ in $Co(OH)_2$. The binding energies for the two peaks in the second group are also well in accordance with standard values related to $Co_{2p1/2sat}$ (803.7 eV) and $Co_{2p3/2sat}$ (787.5 eV) in $Co(OH)_2$. The result agrees well with that obtained in XRD. Besides $Co(OH)_2$, traces of $Co(NO_3)_2$ from the electrolyte also remain in the deposit due to the appearance of the two peaks situated at 781.0 eV and 796.3 eV in the third group. In terms of the XPS results, the contents of Co from different compounds can be calculated using the following Equation (1):

$$C_x = \frac{\rho_x}{\sum_i \rho_i} = \frac{I_x/S_x}{\sum_i I_i/S_x} \quad (1)$$

where C_x is the atomic concentration of the element x, ρ is the atomic density, I is the intensity for the corresponding peak, and S is the relative atomic sensitivity factor.

The calculated results demonstrate that the contents of Co in $Co(OH)_2$ and $Co(NO_3)_2$ are 96.03 *w*/% and 3.97 *w*/%, respectively. Then, the contents of the corresponding compounds containing Co can be further estimated at about 92.42 *w*/% for $Co(OH)_2$ and 7.58 *w*/% for $Co(NO_3)_2$. It is clear that the high-purity $Co(OH)_2$ deposits were successfully synthesized in this study.

SEM was using to characterize the evolution in morphology of the deposits with the introduction of RGO and the change in applied potential. **Figure 4** demonstrates the change in surface morphology of NF before and after the deposition of GO. A large number of equiaxed grains are uniformly distributed throughout the whole surface of NF before the electrophoretic deposition (**Figures 4a** and **4b**). However, a layer of the fold-like deposits adheres to the surface of NF after the electrophoretic deposition, resulting in the initial grain boundaries being hardly visible (**Figures 4c** and **4d**). It can be concluded that GO is evenly prepared on NF. **Figure 5** indicates the evolution in morphology of the deposits prepared at different potentials. When the potential is –0.75 V, the deposit presents a honeycomb-like structure, in which a large number of nanosheets with a thickness of about 30-80 nm grow without orientation from the RGO surface and connect with each other. Tremendous pores are formed among the nanosheets.

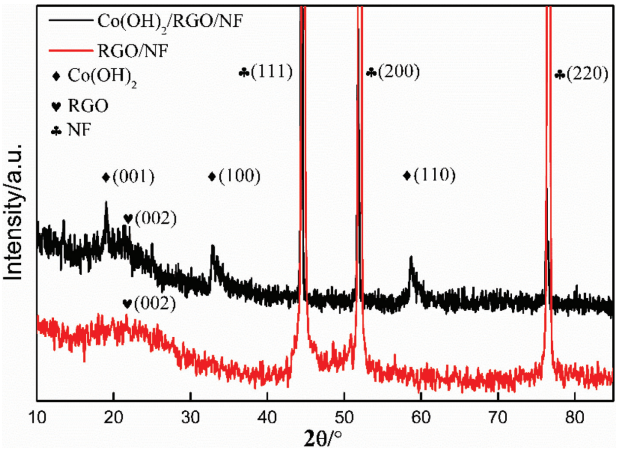

Figure 2: XRD patterns of the RGO/NF before and after the electrodeposition

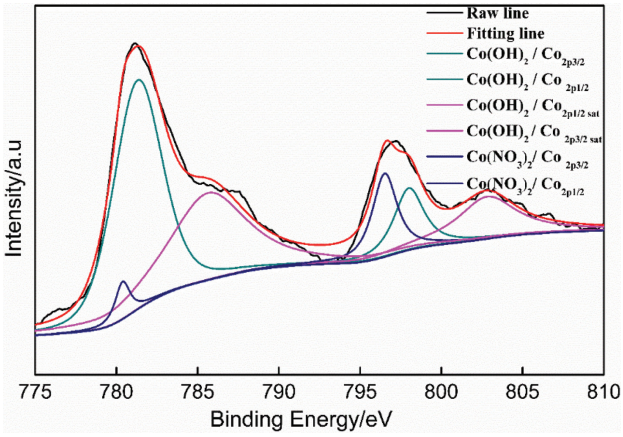

Figure 3: High-resolution XPS spectrum of Co_{2p} in the deposit prepared at –0.85 V

With the potential enhanced to –0.85 V, there is an obvious change in the morphology of the deposit. The deposit becomes denser due to finer nanosheets protruding from the initial pores, which greatly improves the number of pores and reduces their diameters. However, along with the increase to –0.95 V in the applied potential, the deposit becomes very dense, so that there are hardly pores observed in the deposit.

It is clear that the applied potential plays an essential role in the final morphologies of the deposits. With the increase in potential, the nanosheets involved in the deposit become finer, accompanied with the gradual densification of the deposit. The former is closely associated with the change in the nucleation rate with the potential. The latter results from the change in growth rate with the potential. It is well known that the potential as the driving force is responsible for the nucleation and subsequent crystal growth. The relationship between nucleation rate and potential can be clearly described by the following Equation (2):

$$\omega = K \exp\left(-\frac{\pi h \sigma_1^2 LA}{\rho nFRT\eta}\right) \tag{2}$$

in which K is the pre-exponential factor, h represents the height of the formed crystal nucleus, σ_1 signifies the interfacial tension between crystal nucleus and solution, L, F and R are the Avogadro constant, Faraday constant and gas constant, A and ρ denote the relative molecular weight and density of the deposit, n is regarded as the transfer charge number during the electrode reactions, T represents the temperature and η denotes the overpotential.

It is clear that the nucleation rate can be greatly improved at a high overpotential, which will contribute to the fineness of the deposit. The crystal growth rate can be associated with the overpotential using the Faraday law as follows:

$$I = nFr_e \tag{3}$$

where I is the current density and r_e represents the reaction rate.

The current is proportional to the overpotential, and the reaction rate characterizes the crystal growth rate. Therefore, a high depositing rate can be acquired at a high overpotential.

Based on the above analyses, it can be concluded that the increase in potential will be beneficial to refining the grains in the deposit, and accelerating the densification of the deposit, which is completely in accordance with the above-mentioned results. The evolution in morphology with the potential can be described as follows. When a low potential is applied (–0.75 V), a large number of nuclei are formed on the surfaces of the RGO (mainly at the steps formed on fold-shaped RGO). Along with the electrode reactions gradually processing, the atoms are constantly integrated into the nuclei (especially the

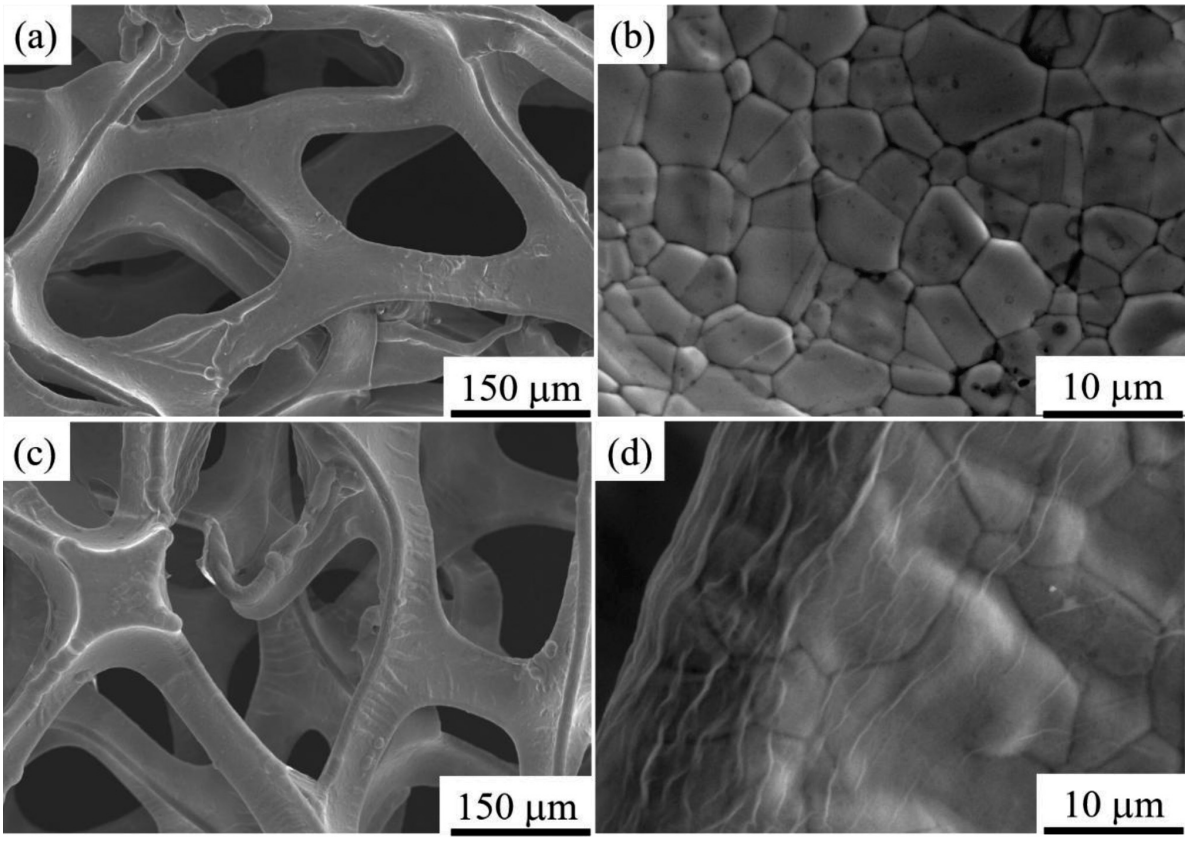

Figure 4: SEM images of: NF (a, b) and RGO/NF (c, d)

defects such as vacancies, dislocations and crystal steps located on the surfaces of nuclei). The nuclei preferentially grow along the direction parallel to the electric field, resulting in the formation of flake grains. The grains are comparatively coarse and considerable pores among the nanosheets are formed due to the low potential. With the potential enhanced to -0.85 V, more nuclei are formed and grow with a faster rate. The grains become finer and the pores are also greatly reduced in terms of volume fraction. When the potential is further increased to -0.95 V, the pores are almost occupied with the overgrowth grains. Obviously, the change in morphology is responsible for the specific surface area of the deposit. The honeycomb-like structure obtained at –0.85 V, composed of numerous fine nanosheets and pores, possesses the highest specific surface area among the three deposits. The structure will be beneficial to the further improvement in electrochemical performance of the electrode as analyzed in the latter.

The effect of the introduction of RGO on the morphologies of the deposits was investigated by SEM. **Figure 6** demonstrates the morphologies of the deposit prepared on NF and RGO/NF by the electrodeposition, which are all acquired under optimum deposition conditions. Comparatively speaking, the introduction of RGO significantly improves the specific surface area of the deposit. RGO with a very high surface area will provide more sites for the heterogeneous nucleation of the deposit. Along with more nuclei formed, their growth spaces will be seriously restricted, resulting in finer nanosheets formed when compared with those without the introduction of RGO.

The above analyses confirm that the applied potential and the introduction of RGO are all crucial to the evolution in morphology of the deposit. Which is the decisive factor can be confirmed by their contribution to the increase in specific capacitance of the deposit as analyzed in 3.2 Electrochemical performance measurement.

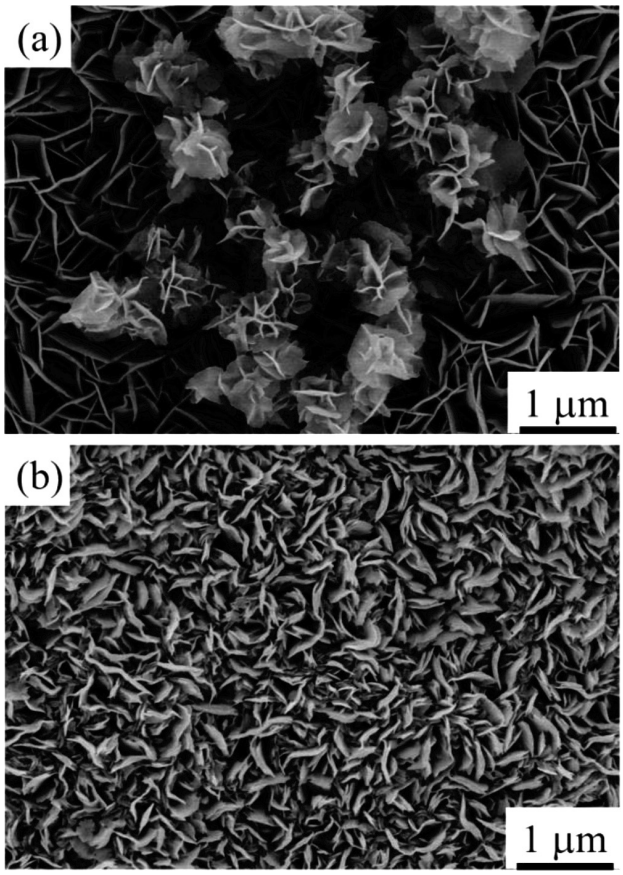

Figure 6: SEM images of: a) $Co(OH)_2$ deposited on NF and b) RGO/NF

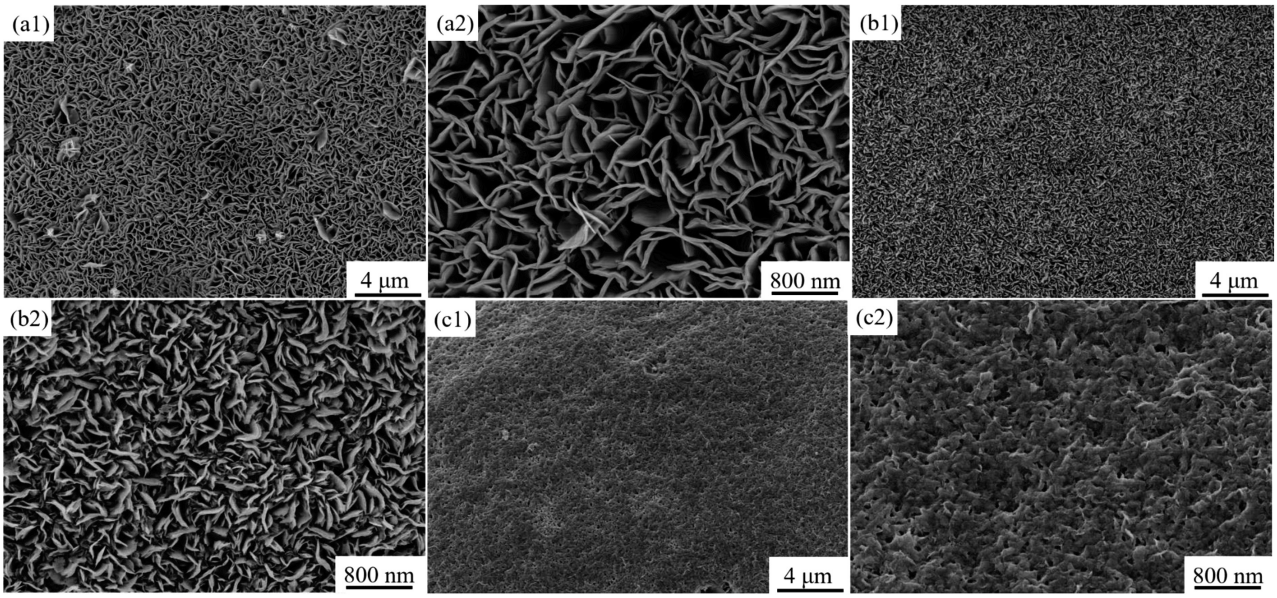

Figure 5: SEM images of: $Co(OH)_2$/RGO/NF prepared at different potentials of: (a1, a2) –0.75 V, (b1, b2) –0.85 V, (c1, c2) –0.95 V

3.2 Electrochemical performance measurement

The specific capacitance of the $Co(OH)_2$/RGO/NF electrode was measured by CV in a 2 mol·L^{-1} KOH electrolyte. In **Figure 7**, the CV curves of all the electrodes at a scanning rate of 5 mV·s^{-1} deviate from the standard rectangle, which implies that the electrodes demonstrate the typical pseudo-capacitance behavior. Besides the pseudo-capacitance originating from $Co(OH)_2$, the electrical double layer capacitance from RGO as a carrier with a high specific surface area is also an essential part involved in the capacitance. Two pairs of redox peaks can be clearly observed during the whole scanning, a pair of redox peaks can be observed at about 0.033 V and –0.044 V, the others are located at around 0.262 V and 0.175 V, indicating that two reversible oxidation and reduction reactions connected with $Co(OH)_2$ occur during the charge and discharge. They can be described as follows:[25–26]

$$Co(OH)_2 + OH^- \rightleftharpoons COOH + H_2O + e^- \quad (4)$$

$$CoOOH + OH^- \rightleftharpoons CoO_2 + H_2O + e^- \quad (5)$$

The integrated area of the CV curves is closely associated with the capacitance of the electrodes, between which a positive correlation relation can be established. Obviously, the capacitance of the electrode prepared at –0.85 V is the largest when compared with that of the other two electrodes due to the largest area surrounded by the CV curve (**Figure 7a**). The specific capacitance can be calculated according to the following formula:

$$C_m = \frac{\int i\mathrm{d}v}{2 \times m \times S \times \Delta V} \quad (6)$$

in which C_m (F·g^{-1}) is the calculated specific capacitance by CV tests, $\int i\mathrm{d}v$ is the area enclosed by the CV curve and calculated by the integral method, m (g) is the mass of the deposited material, ΔV (V) is the scanning potential range, and S (V·s^{-1}) is the scanning rate of the CV tests.

The results are indicated in **Table 1**, where the specific capacitance of the electrode prepared at –0.85 V reaches 1051.2 F·g^{-1} at the scanning rate of 5 mV·s^{-1}, which is far higher than those obtained at the other electrodes (503.4 F·g^{-1} at –0.75 V and 445.7 F·g^{-1} at –0.95 V). The calculated results at the other scanning rates also confirm the conclusion (**Table 1**). It is worth noting that the specific capacitance of all the electrodes presents a declining tendency with the increasing the scanning rate (**Figure 7b**). The specific capacitance of the deposit prepared at –0.85 V is reduced by about 30 % (5 mV·s^{-1}), 38 % (7 mV·s^{-1}) and 40 % (9 mV·s^{-1}) when compared with the value obtained at 3 mV·s^{-1}. A similar phenomenon was also observed for the deposits prepared at –0.75 V and –0.95 V. However, a comparatively high specific capacitance of about 892.2 F·g^{-1} is still retained for the electrode prepared at –0.85 V, which is twice as high as those of the other two electrodes. The specific capacitance of $Co(OH)_2$ directly deposited on NF at the optimal parameters was also measured using CV tests with a scanning rate of 5 mV·s^{-1}, which is only 836 F·g^{-1} (about 80 % of the value for $Co(OH)_2$/RGO/NF prepared at –0.85 V). The result clearly demonstrates that the introduction of RGO will contribute to the improvement in electrochemical performance of the $Co(OH)_2$/NF electrode.

Similar results were acquired using the galvanostatic charging/discharging technique. As shown in **Figure 8**, those profiles are slightly deviating from a typical symmetrical triangle due to two pairs of charge-discharge platforms clearly observed, which derive from two reversible reactions mentioned in the CV tests. The specific capacitance of the $Co(OH)_2$/RGO/NF electrode can be calculated using the following Equation (7):

$$C_m = \frac{I \times \Delta t}{m \times \Delta V} \quad (7)$$

C_m (F·g^{-1}) is the specific capacitance data calculated by constant current charge-discharge method represented, I (A) is the current of GCD, m (g) the mass of $Co(OH)_2$ in supercapacitor, V (V) is the potential range and t (s) is the discharge time.

As shown in **Table 1**, the specific capacitance of the electrodes prepared at –0.75 and –0.95 is about 638.3 F·g^{-1} and 523.2 F·g^{-1} at a current density of 1 A·g^{-1}, which is only half of that prepared at –0.85 V (**Figure 8a**). When the current density is increased from 1 A·g^{-1} to 10 A·g^{-1}, the specific capacitance of the electrode prepared at –0.85 V is decreased by about 23.2 % (1.5 A·g^{-1}), 25.6 % (2.0 A·g^{-1}), 26.4 % (2.5 A·g^{-1}) and 28.7 % (4.0 A·g^{-1}), when compared with that obtained at 1 A·g^{-1} (**Figure 8b**). The specific capacitance of the electrode prepared at –0.85 is about 910.5 F·g^{-1} at a high current density of 4 A·g^{-1}, which is about two to three times that prepared at –0.75 V and –0.95 V (317.1 F·g^{-1} and 411.6 F·g^{-1}). The specific capacitance of the $Co(OH)_2$/NF electrode was also measured by the galvanostatic charging/discharging technique. The highest value is about 725 F·g^{-1} obtained at a current density of 4 A·g^{-1}, which is also about 80 % of the highest value obtained at the $Co(OH)_2$/RGO/NF electrode. The positive role of the introduction of RGO in the improvement of electrochemical performance of $Co(OH)_2$/NF electrodes is further confirmed.

The mass-specific capacitance can only characterize the stored charges of unit mass, which does not signify the total stored charges since it is also related to the total mass. The shortcoming involved in mass-specific capacitance can be resolved by introducing the other indicator named as the area-specific capacitance, which is related to not only the mass specific capacitance, but also the total mass of the deposited active substance of unit area. Therefore, the area-specific capacitance of those deposits acquired at different potentials is also

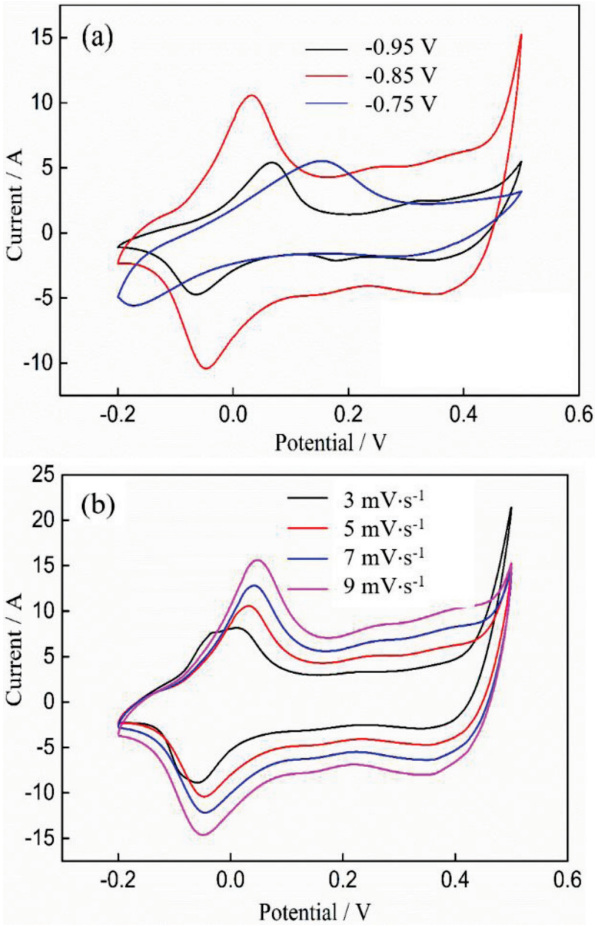

Figure 7: CV curves recorded on the $Co(OH)_2$/RGO/NF electrodes; a) the electrodes prepared at different potentials at a scanning rate of 5 $mV \cdot s^{-1}$, b) the electrode at –0.85 V at different scanning rates

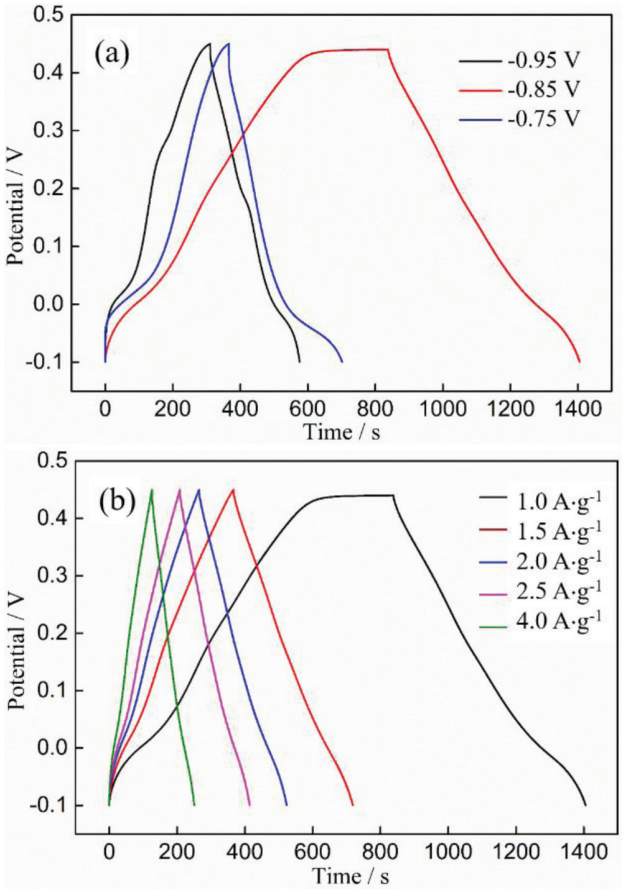

Figure 8: Galvanostatic charge/discharge curves recorded on the $Co(OH)_2$/RGO/NF electrodes: a) the electrodes prepared at different potentials at a current density of 1 $A \cdot g^{-1}$, b) the electrode at –0.85 V at different current densities

provided (**Table 1**). Obviously, the area-specific capacitance of the deposit obtained at –0.85 V is also much higher than that of the deposits obtained at –0.75 and –0.95 V, whether for CV or for galvanostatic charge/discharge tests (15.2 $F \cdot cm^{-2}$ for –0.85 V, 1.6 $F \cdot cm^{-2}$ for –0.75 V and 5.9 $F \cdot cm^{-2}$ for –0.95 V at 3 $mV \cdot s^{-1}$ in CV tests; (12.9 $F \cdot cm^{-2}$ for –0.85 V, 1.7 $F \cdot cm^{-2}$ for –0.75 V and 5.8 $F \cdot cm^{-2}$ for –0.95 V at 1.0 $A \cdot g^{-1}$ in galvanostatic charge/discharge tests). This further confirms that the deposit acquired at –0.85 V exhibits the best electrochemical performance.

For the $Co(OH)_2$ electrode, the charges are mainly stored by means of the reversible oxidation-reduction reactions, which can be divided into two categories: rapid adsorption and desorption of cations located on the surface of an active substance and the insertion and desertion of cations located in the interior of the active substance. Therefore, the specific capacitance is closely associated with the morphology of the prepared active substance. As shown in **Figure 5**, the deposit prepared at –0.85 V is composed of finer nanosheets, among which more pores with smaller diameter are formed. The honeycomb-like structure has the higher specific surface when compared with that formed at –0.75 and –0.95 V. The electrolyte can rapidly diffuse into the interior of the active substance by means of numerous fine pores, sufficiently in contact with more nanosheets, and participate in the electrode reactions occurring on the surface of an active substance. This contributes to the improvement in specific capacitance. Moreover, for the inner of nanosheets, finer nanosheets will greatly shorten the transportation distance of inner cations, which is also beneficial to the improvement in specific capacitance due to the acceleration in electrode reaction. For the deposit prepared at –0.75 V, the specific surface is comparatively low due to the formed coarse grains, resulting in fewer cations on the surface of the active substance involved in the electrode reactions. Besides that, coarse grains will retard the migration of cations in the inner of the active substance. The two factors cause the decrease in the specific capacitance of the deposit prepared at –0.75 V. For the deposit obtained at –0.95 V, although the grains become finer, their overgrowth makes them connect with each other, leaving a few pores remaining. The change

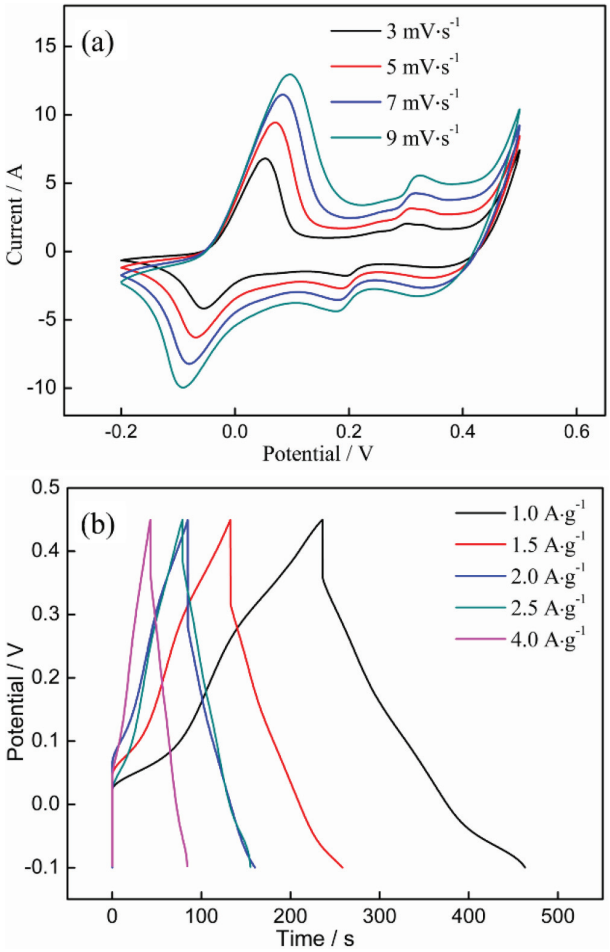

Figure 9: a) CV curves recorded on the $Co(OH)_2$/NF electrode prepared at -0.85 V at different scanning rates, b) galvanostatic charge/discharge curves recorded on the $Co(OH)_2$/NF electrode prepared at -0.85 V at different current densities

not only reduces the specific surface area, but also retards the migration of the inner cations, so that the specific capacitance is also comparatively low. Based on the above analyses, a suitable applied potential would be –0.85 V.

Table 1: Specific capacitance of $Co(OH)_2$/RGO/NF composite electrode calculated by CV and galvanostatic charge/discharge (GCD) at different deposition potentials

Samples		–0.75 V/ F·g^{-1}	–0.75 V/ F·cm^{-2}	–0.85 V/ F·g^{-1}	–0.85 V/ F·cm^{-2}	–0.95 V/ F·g^{-1}	–0.95 V/ F·cm^{-2}
CV	3 mV·s^{-1}	590.1	1.6	1503.8	15.2	528.1	5.9
	5 mV·s^{-1}	503.4	1.4	1051.2	10.6	445.7	5.0
	7 mV·s^{-1}	453.2	1.2	931.7	9.4	414.7	4.6
	9 mV·s^{-1}	410.3	1.1	892.2	9.0	398.1	4.4
GCD	1.0 A·g^{-1}	638.2	1.7	1277.5	12.9	523.2	5.8
	1.5 A·g^{-1}	573.8	1.5	980.5	9.9	482.0	5.4
	2.0 A·g^{-1}	522.5	1.4	950.9	9.6	462.9	5.2
	2.5 A·g^{-1}	474.5	1.3	940.0	9.5	448.0	5.0
	4.0 A·g^{-1}	317.1	0.8	910.5	9.2	411.6	4.6

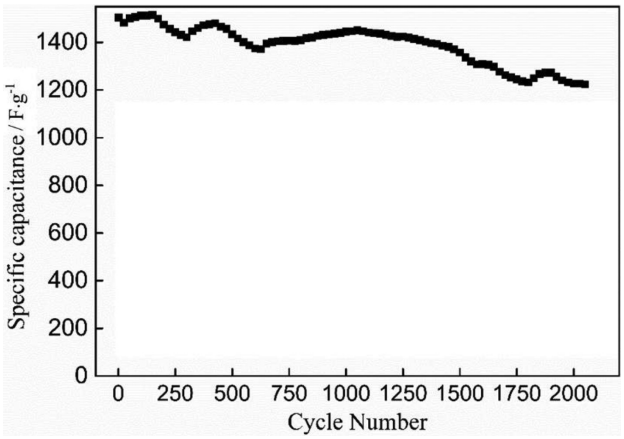

Figure 10: CV tests for $Co(OH)_2$/RGO/NF prepared at –0.85 V at 5 mV·s^{-1} up to 2000 cycles

In order to reveal the effect of the introduction of RGO on the electrochemical performance, the specific capacitance of the $Co(OH)_2$//NF electrode prepared at –0.85 V was also measured by CV and a galvanostatic charging/discharging technique (**Figure 9**). The results indicate that the mass and area-specific capacitances are much lower than those obtained in the $Co(OH)_2$/RGO//NF electrode. This proves that the introduction of RGO is also the other decisive factor affecting the electrochemical performance besides the applied potential. The introduction of RGO with a large specific surface area will contribute to refining the grains of the deposit by providing more heterogeneous nucleation sites, which will be in favor of an improvement in the specific capacitance due to the increase in the number of cations of unit mass. Moreover, the RGO with superior conductivity will promote the migration of charges, which is also conducive to an enhancement in the specific capacitance.

$Co(OH)_2$/RGO/NF prepared at –0.85 V with a highest specific capacitance was selected to measure the cycling stability by CV (2000 cycles were carried out at a scanning rate of 5 mV·s^{-1} with a potential range from –0.2 V to 0.5 V). The relationship between the specific capacitance and the cycling number is shown in **Figure 10**. After 2000 cycles, the specific capacitance is 1222 F·g^{-1} and the capacity retention rate is 83 %, which also implies that the electrode possesses an excellent cycling stability.

4 CONCLUSIONS

1) $Co(OH)_2$ nanosheets with a high specific surface area were prepared on RGO/NF by a combination of electrophoretic deposition followed by thermal reduction, and electrodeposition.

2) The applied potential played an essential role in the morphological evolution of the deposits. $Co(OH)_2$ nanosheets prepared at a low potential of –0.75 V were

comparatively coarse and a large number of pores were formed among the nanosheets. $Co(OH)_2$ nanosheets prepared at a high potential of –0.95 V overgrew and connected with each other, resulting in a dramatic reduction in the number of pores. Finer $Co(OH)_2$ nanosheets with a highest specific surface were deposited at –0.85 V due to more pores with a smaller diameter being formed.

3) The specific capacitance of the $Co(OH)_2$/RGO/NF electrodes was closely related to the morphologies of $Co(OH)_2$. The highest specific capacitance was obtained in the electrode prepared at –0.85 V (1503.8 $F \cdot g^{-1}$ and 15.2 $F \cdot cm^{-2}$ at 3 $mV \cdot s^{-1}$ for CV, 1277.5 $F \cdot g^{-1}$ and 12.9 $F \cdot cm^{-2}$ at 1 $A \cdot g^{-1}$ for galvanostatic charge/discharge). The electrode also demonstrated an excellent cycling stability (the specific capacitance loss was about 17 % after 2000 CV tests).

Acknowledgment

This work was financially supported by the National Natural Science Foundation of China, China (51471105), "Shu Guang" project of Shanghai Municipal Education Commission and Shanghai Education Development Foundation (12SG44).

5 REFERENCES

[1] F. Y. Cheng, J. Chen, Something from nothing. Nature Chemistry. 4 (**2012**) 962–963, doi:10.1038/nchem.1516

[2] M. K. Debe, Electrocatalyst approaches and challenges for automotive fuel cells, Nature 486 (**2012**) 43–51, doi:10.1038/nature11115

[3] M. Armand, J. M. Tarascon, Building better batteries, Nature, 451 (**2008**) 652–657, doi.org/10.1038/451652a

[4] X. Peng, L. L. Peng, C. Z. Wu, Y. Xie, Two dimensional nanomaterials for flexible supercapacitors, Chemical Society Reviews, 43 (**2014**) 3303–3323, doi:10.1039/c3cs60407a

[5] Y. Zhu, S. Murali, M. D. Stoller, K. J. Ganesh, W. Cai, P. J. Ferreira, A. Pirkle, R. M. Wallace, K. A. Cychosz, M. Thommes, D. Su, Carbon-based supercapacitors produced by activation of graphene, Science 332 (**2011**) 1537–1541, doi:10.1126/science.1200770

[6] S. Zheng, X. Li, B. Yan, Q. Hu, Y. Xu, X. Xiao, H. Xue, H. Pang, Transition-metal (Fe Co, Ni) based metal-organic frameworks for electrochemical energy storage, Advanced Energy Materials 7 (**2017**) 1602733, doi:10.1002/aenm.201602733

[7] Y. Q. Zhang, X. H. Xia, X. L. Wang, Y. J. Mai, S. J. Shi, Y. Y. Tang, L. Li, J. P. Tu, Silicon/graphene-sheet hybrid film as anode for lithium ion batteries. E Electrochemistry Communications, 23 (**2012**) 17–20, doi:10.1016/j.elecom.2012.07.001

[8] Y. N. Xia, P. D. Yang, Y. Sun, Y. B. Wu, B. Mayers, Y. Gates, F. Yin, H. Kim, Yan One-Dimensional Nanostructures: Synthesis, Characterization, and Applications, Advanced Materials, 15 (**2003**) 353–389, doi:10.1002/chin.200322236

[9] X. H. Xia, J. P. Tu, Y. Q, Zhang, Y. J. Mai, X. L. Wang, C. D. Gu, X. B. Zhao, Three-dimentional porous nano-Ni/$Co(OH)_2$ nanoflake composite film: a pseudocapacitive material with superior performance, Journal of Physical Chemistry C, 115 (**2011**) 22662–22668, doi:10.1021/jp208113j

[10] M. Li, S. H. Xu, C Cherry, Y. P. Zhu, P. X. Yang, L W Wang, P. K. Chu, Asymmetrical Supercapacitor Composed of Thin Co(OH)2 Nanoflakes on Three-Dimensional Ni/Si Microchannel Plates with Superior Electrochemical Performance, Electrochimica Acta, 149, 18–27, doi:10.1016/j.electacta.2014.10.091

[11] D. Ghosh, S. Giri, C.K. Das, Preparation of CTAB assisted hexagonal platelet $Co(OH)_2$/graphene hybrid composite as efficient supercapacitor electrode material, ACS Sustainable Chemistry & Engineering, 1 (**2013**) 1135, doi:10.1021/sc400055z

[12] C. Zhou, Y. Zhang, Y. Li, J. Liu, Construction of High-Capacitance 3D CoO@Polypyrrole Nanowire Array Electrode for Aqueous Asymmetric Supercapacitor. Nano letters, 13 (**2013**) 2078–2085, doi:10.1021/nl400378j

[13] C. M. Zhao, X. Wang, S. M. Wang, Y. Y. Wang, Y. X. Zhao, W. T. Zheng. Synthesis of $Co(OH)_2$/graphene/Ni foam nano-electrodes with excellent pseudocapacitive behavior and high cycling stability for supercapacitors. International Journal of Hydrogen Energy, 37 (**2012**) 11846–11852, doi:10.1016/j.ijhydene.2012.05.138

[14] U. M. Patil, M. S. Nam, J. S. Sohn, S. B. Kulkarni, R. Shin, S. Kang, S. Lee, J. H. Kim, S. C. Jun, Controlled electrochemical growth of $Co(OH)_2$ flakes on 3D multilayered graphene foam for high performance supercapacitors, Journal of Materials Chemistry A, 2 (**2014**) 19075–19083, doi:10.1039/c4ta03953j

[15] D. Zhang, W. Zou, Synthesis and characterization of $Co(OH)_2$/graphene as supercapacitor materials, International Journal of Materials Research, 106 (**2015**) 72–75, doi:10.3139/146.111148

[16] E. M. Jin, H. J. Lee, H. B. Jun, S. M. Jeong, Electrochemical properties of α-$Co(OH)_2$/graphene nano-flake thin film for use as a hybrid supercapacitor, Korean Journal of Chemical Engineering, 34 (**2017**) 885–891, doi:10.1007/s11814-016-0323-z

[17] A. D. Jagadale, V S Kumbhar, D. S. Dhawale, C. D. Lokhande, Potentiodynamically deposited nickel oxide (NiO) nanoflakes for pseudocapacitors, Journal of Electroanalytical Chemistry, 704 (**2013**) 90–95, doi:10.1016/j.jelechem.2013.06.020

[18] W. J. Zhou, J. Zhang, T. Xue. Electrodeposition of ordered mesoporous cobalt hydroxide film from lyotropic liquid crystal media for electrochemical capacitors. Journal of Materials Chemistry, 18 (**2008**) 905–910, doi:10.1039/B715070A

[19] S. Ghasemi, R. Hosseinzadeh, M. Jafari, MnO_2 nanoparticles decorated on electrophoretically deposited graphene nanosheets for high performance supercapacitor. International Journal of Hydrogen Energy, 40 (**2015**) 1037–1046, doi:10.1016/j.ijhydene.2014.11.072

[20] Y. H. Xu, J Li. W. X. Huang, Porous Graphene Oxide Prepared on Nickel Foam by Electrophoretic Deposition and Thermal Reduction as High-Performance Supercapacitor Electrodes, Materials, 10 (**2017**) 936, doi:10.3390/ma10080936

[21] C. Xiong, T. Li, Y. Zhu, T. Zhao, A. Dang, H. Li, X. Ji, Y. Shang, M. Khan, Two-step approach of fabrication of interconnected nanoporous 3D reduced graphene oxide-carbon nanotube-polyaniline hybrid as a binder-free supercapacitor electrode, Journal of Alloys and Compounds, 695 (**2017**) 1248–1259, doi:10.1016/j.jallcom.2016.10.253

[22] C. Deng, J. Jiang, F. Liu, L. Fang, J. Wang, D. Li, J. Wu, Influence of graphene oxide coatings on carbon fiber by ultrasonically assisted electrophoretic deposition on its composite interfacial property, Surface and Coatings Technology, 272 (**2015**) 176–181, doi:10.1016/j.surfcoat.2015.04.008

[23] S.Y. Huang, G. P. Wu, C. M. Chen, Y. Yang, S. C. Zhang, C. X. Lu. Electrophoretic deposition and thermal annealing of a graphene oxide thin film on carbon fiber surfaces, Carbon, 52 (**2013**) 605–620, doi.org/10.1016/j.carbon.2012.09.062

[24] C. F. Wang, J. Li, S. F. Sun, X. Y. Li, F. Zhao, B. Jiang, Y. D. Huang, Electrophoretic deposition of graphene oxide on continuous carbon fibers for reinforcement of both tensile and interfacial strength, Composites Science And Technology, 135 (**2016**) 46–53, doi:10.1016/j.compscitech.2016.07.009